HHS Public Access

Author manuscript

Macromol Biosci. Author manuscript; available in PMC 2023 July 24.

Published in final edited form as:

Macromol Biosci. 2023 July ; 23(7): e2300011. doi:10.1002/mabi.202300011.

In Vitro Proof of Concept of a First-Generation Growth-Accommodating Heart Valved Conduit for Pediatric Use

Dr. Richard L. Li[a,b], **Dr. Mingze Sun**[a], **Dr. Jonathan B. Russ**[c], **Dr. Pierre-Louis Pousse**[a], **Dr. Alexander P. Kossar**[a], **Dr. Isabel Gibson**[a], **Costas Paschalides**[b], **Abigail R. Herschman**[a,b], **Dr. Maryam H. Abyaneh**[a], **Prof. Giovanni Ferrari**[a], **Dr. Emile Bacha**[a], **Prof. Haim Waisman**[c], **Prof. Vijay Vedula**[b], **Prof. Jeffrey W. Kysar**[b,d], **Dr. David Kalfa**[a]

[a]Department of Surgery, Division of Cardiac, Thoracic and Vascular Surgery, Section of Pediatric and Congenital Cardiac Surgery, New-York Presbyterian - Morgan Stanley Children's Hospital, Columbia University Medical Center, 3959 Broadway, CHN-274, New York, NY 10032 USA

[b]Department of Mechanical Engineering, Fu Foundation School of Engineering and Applied Science, Columbia University, 220 Mudd Building, 500 W. 120th Street, New York, NY 10027 USA

[c]Department of Civil Engineering and Engineering Mechanics, Fu Foundation School of Engineering and Applied Science, Columbia University, 610 Mudd Building, 500 W. 120th Street, New York, NY 10027 USA

[d]Department of Otolaryngology – Head and Neck Surgery, Columbia University Medical Center, 3959 Broadway, 5th Floor, New York, NY 10032 USA

Abstract

Currently available heart valve prostheses have no growth potential, requiring children with heart valve diseases to endure multiple valve replacement surgeries with compounding risks. This study demonstrates the *in vitro* proof of concept of a biostable polymeric trileaflet valved conduit designed for surgical implantation and subsequent expansion via transcatheter balloon dilation to accommodate the growth of pediatric patients and delay or avoid repeated open-heart surgeries. The valved conduit is formed via dip molding using a polydimethylsiloxane-based polyurethane, a biocompatible material shown here to be capable of permanent stretching under mechanical loading. The valve leaflets are designed with an increased coaptation area to preserve valve competence at expanded diameters. Four 22 mm diameter valved conduits are tested *in vitro* for hydrodynamics, balloon dilated to new permanent diameters of 23.26 ± 0.38 mm, and then tested again. Upon further dilation, two valved conduits sustain leaflet tears, while the two surviving devices reach final diameters of 24.38 ± 0.19 mm. After each successful dilation, the valved

Corresponding authors' information: Dr. D. Kalfa, MD, PhD, Pediatric Cardiac Surgery, New-York Presbyterian - Morgan Stanley Children's Hospital, Columbia University Medical Center, 3959 Broadway, CHN-274, New York, NY 10032 USA, Tel.: (212) 305-5975; fax: (212) 305-4408, dk2757@cumc.columbia.edu; Prof. J. W. Kysar, PhD, Department of Mechanical Engineering, Columbia University, 240 Mudd Building, Mail Code 4703, 500 W. 120th Street, New York, NY 10027 USA, Tel.: (212) 854-7432; fax: (212) 854-3304, jk2079@columbia.edu.

Supporting Information

Supporting Information is available from the Wiley Online Library or from the authors.

Conflict of Interest Statement

The authors declare no conflicts of interest or relationships with industry.

conduits show increased effective orifice areas and decreased transvalvular pressure differentials while maintaining low regurgitation. These results demonstrate concept feasibility and motivate further development of a polymeric balloon-expandable device to replace valves in children and avoid reoperations.

Graphical Abstract

We report the *in vitro* proof of concept of a biostable polymeric valved conduit, designed to accommodate growth via transcatheter balloon dilation. Four devices are initially expanded from 22 to 23.26 mm in diameter. Two devices are further dilated to 24.38 mm, while the remaining two sustain leaflet tears. The surviving devices demonstrate increased orifice areas and decreased transvalvular gradients.

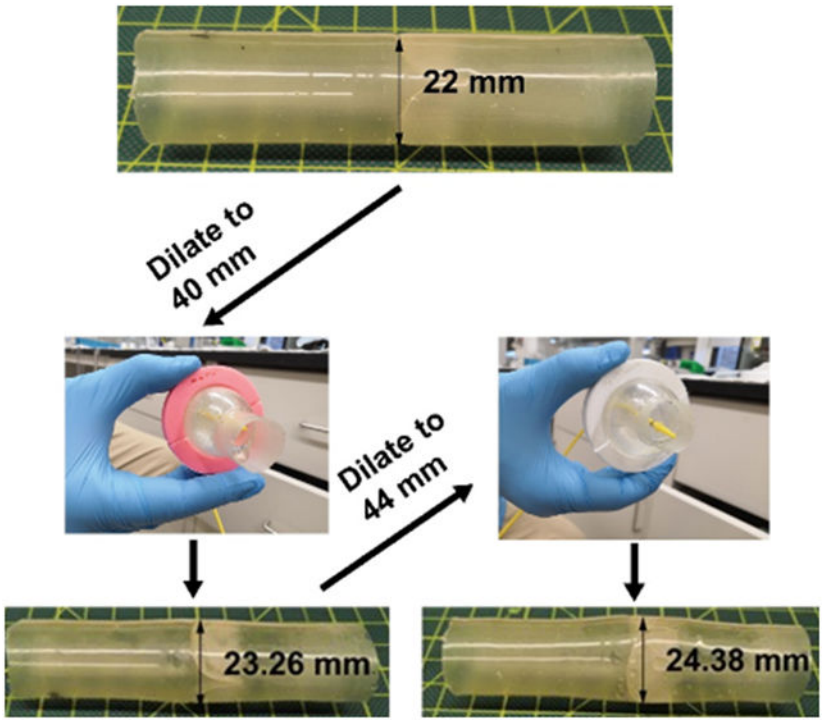

Keywords

growth accommodation; valved conduit; polymeric valves; right ventricular outflow tract; congenital heart disease

1 Introduction

Congenital heart disease (CHD) is reported in approximately 1% of all live births, affecting ~40,000 babies per year in the U.S. and ~1.4 million worldwide.[1] Common conditions associated with CHD include atrial and ventricular septal defects (holes in the internal walls of the heart), aortic and pulmonary stenoses (narrowing of the valves and arteries), and tetralogy of Fallot (a combination of a ventricular septal defect, pulmonary stenosis, right ventricular hypertrophy, and an overriding aorta).[2] More than half of children born with

CHD require open-heart surgery to correct these malformations, and more than 20% of those who require surgery will need the implantation of a valve or valved conduit to repair the right ventricular outflow tract (RVOT).[1,3,4]

However, all currently available valved prostheses, including cryopreserved homografts, xenograft conduits, bioprostheses, and mechanical prostheses, have serious limitations resulting in high rates of reintervention.[5,6] Tissue valves exhibit poor durability due to structural valve degeneration (SVD), which encompasses thickening, calcification, tearing, or other disruptions to the leaflet tissue leading to stenosis or regurgitation.[7-10] Mechanical valves do not degrade substantially, but they are susceptible to obstruction from pannus formation.[11] Other drawbacks of mechanical valves include their larger size, which limits their use in younger patients,[6] and their hinged design, which creates non-physiological flow patterns that increase the risk of thrombosis and necessitate anticoagulation therapy.[12] Most critically, all these devices are designed to function at a fixed size and are constructed from non-living tissue or rigid materials that do not adapt to the patient's somatic growth. As a result of these limitations, children with prosthetic valves require one to four reoperations to replace the valve before they reach adulthood,[11,13,14] with each additional open-heart surgery carrying a 1-15% risk of death, bleeding, infection or multi-organ dysfunction.[5,15,16]

Commonly reported reasons for reoperations in pediatric patients include somatic outgrowth,[11,17] complications due to SVD in tissue valves (e.g. stenosis, regurgitation),[13,18] and in rarer cases, endocarditis and aneurysm.[11,13] Both outgrowth and SVD can occur independently, as SVD is a common occurrence even in fully grown adults.[8,9] However, SVD has been shown to be accelerated in children, with an increase in the frequency of required reoperations.[18-20] While this phenomenon has been attributed to intensified immunological responses, altered blood biochemistry, and increased calcium metabolism,[21,22] another possible mechanism driving acceleration of SVD is outgrowth. An outgrown or undersized valve (which is effectively stenotic) creates high pressure gradients and turbulent flow that can trigger a cascade effect: increased internal leaflet stresses, intimal proliferation, macrophage infiltration[22] leading to reactive-oxygen-species-mediated (ROS) oxidation,[23,24] and leaflet thickening resulting in further stress increases, calcification, degradation, and mechanical failure of the valve.[14,22,25-27]

A new valved device that can accommodate a child's growth would reduce the need for reoperations and greatly improve the standard of care for children and adults with CHD. The ideal device will last from the newborn stage well into adulthood, although the elimination of even one reoperation to upsize a valved prosthesis would have a significant clinical impact.

There have been attempts to surgically implant percutaneous stented valves, such as the Melody™ transcatheter pulmonary valve,[28-32] for later intervention by transcatheter balloon dilation. However, these subsequent dilations have occasionally resulted in severe regurgitation[29] because the Melody™ was not originally designed to be competent across a large range of diameters – there is insufficient coaptation area, or leaflet contact, at larger diameters to enable valve closure – or to be expanded multiple times. There

is now an increased focus on developing valved devices specifically to accommodate a child's growth. The Autus Valve (Boston, Massachusetts) is an incrementally balloon-expandable valve mimicking the bileaflet geometry of a human venous valve.[33] Designed for pulmonary valve replacement and growth accommodation in pediatric patients, it is currently undergoing human clinical trials.[34] Meanwhile, Draper Laboratory, Inc. (Cambridge, Massachusetts) is developing the LEAP valve, which has an adaptive stent that expands without the need for balloon interventions.[35]

However, none of these devices are integrated with expandable conduits designed for reconstruction of the RVOT. In more than half of the patients requiring pulmonary valve implantations and in all such neonates, infants, and children up to the age of 5-6 years, the RVOT is entirely absent or insufficiently sized.[36] Thus, a valved conduit is the major clinical need for this population, as a valve-only device would not be adequate to fully reconstruct the RVOT and properly accommodate growth. An expandable valve-only prosthesis could potentially be inserted into an expandable vascular graft. However, such a configuration has not been studied, and the effect of balloon expansion on the cohesion between these separate components is unknown.

We report the first *in vitro* proof of concept of a growth-accommodating polymeric valve with an integrated conduit – a valved conduit – that can be implanted surgically for pediatric RVOT reconstruction and subsequently expanded via transcatheter balloon dilation to match part of the patient's growth into adulthood, thus being suitable for adult patients as well. We hypothesize that the expandability of the device can be achieved by using a permanently deformable polymeric material, in contrast to current mechanical and tissue-based valves, and that valve competence can be maintained at expanded diameters by designing the valve leaflets with an increased coaptation area, where this increased area is obtained by increasing the leaflet coaptation height and free edge length. Our objective here was to select biostable polymers that meet the mechanical requirements, design and fabricate the first generation of a fully polymeric biostable valved conduit, and test it *in vitro* before and after balloon dilations.

2 Results

2.1 Materials Characterization and Selection

Two commercially available, biostable, and biocompatible polymers, Carbothane™ AC-4075A (Lubrizol, Cleveland, Ohio), which is a polycarbonate urethane (PCU), and Elast-Eon™ E5-325 (Biomerics, Salt Lake City, Utah), which is a polydimethylsiloxane-based (PDMS) polyurethane (PU), were identified as potential materials for the valved conduit proof of concept due to their high compliance matching that of native heart valve tissue[37,38] and their excellent biocompatibility.[39-44] Furthermore, Carbothane™ and Elast-Eon™ are known to be processable by dip molding, a fabrication technique which has produced excellent results for polymeric valves.[38,45] These materials were further evaluated by mechanical and biocompatibility testing to determine their suitability for constructing the device.

2.1.1 Mechanical Testing—The objective of the mechanical tests was to assess the capacity of the materials for permanent (inelastic) deformation as a result of stretching under uniaxial mechanical loading. Herein, we refer to the amount of deformation of a sample, whether temporary or permanent, by the stretch ratio $\lambda = L/L_0$, where L is the length of the uniformly deformed sample and L_0 is its initial length. First, to determine the extent to which the materials could be stretched, we obtained their uniaxial elongations at break and ultimate strengths. The Carbothane™ samples ($n = 5$) had an elongation at break of $\lambda_{ult} = 5.81 \pm 0.08$ and a nominal tensile strength of $\sigma_{ult} = 48.40 \pm 2.52$ MPa (mean ± s.d.). The Elast-Eon™ samples ($n = 5$) were stretched to the crosshead travel limit of the tensile testing machine at $\lambda = 6$, but they did not break. The corresponding nominal tensile stress at $\lambda = 6$ was $\sigma = 13.12 \pm 0.27$ MPa.

The time-dependent viscoelastic behaviors of Carbothane™ and Elast-Eon™ ($n = 4$ samples each group) were characterized by uniaxial stress relaxation tests. Averaged results in Figure 1a show that the stress decreased quickly within the first 50 seconds. By 300 seconds, the stress had begun to asymptotically approach a stable limit, indicating that most of the viscoelastic response had dissipated. The remaining stress at the stable limit represents elastic energy being stored. These results provide an estimate of the time scale of the transient viscoelastic behavior in Carbothane™ and Elast-Eon™.

Individual samples of the two materials were each subjected to a single temporary stretch λ_{temp} and allowed to recover. The amount of permanent stretch λ_{perm} remaining after 24 hours was recorded. Since the stress relaxation responses had approached a stable limit within 300 seconds, we determined that 24 hours was long enough to properly account for time-dependent viscous strain. Both Elast-Eon™ and Carbothane™ exhibited elastomeric mechanical behavior, with significant elastic and viscoelastic recovery from large deformations and relatively small amounts of permanent stretch (Figure 1b-c). Stretching Elast-Eon™ by $\lambda_{temp} = 5$ resulted in a permanent stretch of $\lambda_{perm} = 1.49 \pm 0.03$ ($n = 4$, mean ± s.d.) (Figure 1b), while the same test for Carbothane™ resulted in $\lambda_{perm} = 1.36 \pm 0.06$ ($n = 8$) (Figure 1c). Stretching Elast-Eon™ by $\lambda_{temp} = 2$, 3, and 4 resulted in permanent stretches of 1.06 ± 0.03 ($n = 7$), 1.14 ± 0.03 ($n = 7$), and 1.33 ± 0.06 ($n = 5$), respectively. Stretching Carbothane™ by $\lambda_{temp} = 2$, 3, and 4 resulted in permanent stretches of 1.01 ± 0.01 ($n = 4$), 1.04 ± 0.03 ($n = 5$), and 1.31 ± 0.06 ($n = 4$), respectively (Figure 1d).

2.1.2 In Vivo Biocompatibility Testing—The biocompatibility of the following polymers was evaluated in a rat subcutaneous model[46-49] of implantation: 1) non-stretched Carbothane™, 2) non-stretched Elast-Eon™, 3) Elast-Eon™ which had been temporarily stretched by 2x, resulting in a 1.1x permanent pre-stretch, and 4) FDA-approved expanded polytetrafluoroethylene (ePTFE) (GORE® PRECLUDE® Pericardial Membrane, W. L. Gore & Associates, Flagstaff, Arizona) as the control group since multiple ePTFE-based valvular devices are currently used in clinical practice and have shown excellent biocompatibility, biostability and durability.[50-53] Figure 1 shows histological sections of the materials upon explantation after 2 months. The pink color in Figure 1e-h indicates the formation of encapsulating tissue, which is the inevitable host response to the implantation of an artificial material. Figure 1e-l shows that the Carbothane™ and Elast-Eon™ samples had good biocompatibility, displaying a lack of cell penetration (lack of foreign body response)

and lack of calcification (lack of immunological response) similar to the ePTFE control patches. There was also no visible difference between the pre-stretched and non-stretched Elast-Eon™ samples.

The mechanical tests of both Elast-Eon™ and Carbothane™ showed only limited permanent stretch. Nevertheless, Elast-Eon™ retained permanent stretches that were greater than in Carbothane™ (λ_{temp} = 2, p = 0.008; λ_{temp} = 3, p = 5e-5; λ_{temp} = 4, p = 0.65; λ_{temp} = 5, p = 0.0038) and substantial enough to demonstrate the proof of concept of growth accommodation. Elast-Eon™ also demonstrated good biocompatibility and was therefore selected for fabricating the first-generation valved conduit prototype.

2.2 First-Generation Design

The design of the valved conduit comprises a cylindrical conduit with a trileaflet valve located at the center (Figure 2a). The geometry of the valve leaflets is elliptical along the radial direction and hyperbolic along the circumferential direction, following equations previously described by Mackay et al.[54] To ensure the persistence of valve competence at larger diameters after the expansion, this design was modified (SolidWorks, Dassault Systèmes, Waltham, Massachusetts) to have an increased coaptation area. The associated increased coaptation height h was calculated as

$$h = \sqrt{l^2 - b^2}, \tag{1}$$

where h is the height of a right triangle having base length b equal to the initial conduit radius and hypotenuse length l equal to the expanded conduit radius (Figure 2b). The new length of the free edge was set as $2l$ using a triangular profile.

In this study, the valved conduit was designed to have an initial diameter of 22 mm. Since the mechanical tests for Elast-Eon™ showed that λ_{temp} = 2 would produce λ_{perm} = 1.06 ± 0.03, it was calculated that a 44 mm temporary balloon dilation (near the limit of clinical feasibility in adolescents) of the 22 mm device would yield a final diameter of 23.32 mm (λ_{perm} = 1.06). Using b = 11 mm and l = 12 mm (23.32 mm / 2 ≈ 12 mm) in Equation (1), the increased coaptation height was estimated to be h = 4.8 mm. After rounding up to h = 5 mm, l was recalculated as l = 12.1 mm, and the new length of the free edge was $2l$ = 24.2 mm. The length of the conduit was ~9 cm to fit the pulse duplicator testing fixture.

2.3 Fabrication

We used dip molding in Elast-Eon™ to fabricate four 22 mm diameter valved conduit prototypes (Devices #1-4) (Figure 2c). The resulting conduit wall and leaflet thicknesses are shown in Figure 3. There was some variation in these thicknesses along the length of the device, as expected from the flow of synthetic polymer solution with the dip molding technique.

2.4 *In Vitro* Evaluation

The four valved conduits were tested *in vitro* for hydrodynamics in a heart valve pulse duplicator, successively dilated to larger diameters, and tested again after each dilation

for hydrodynamics. The devices were dilated using a Coda balloon catheter first to a maximum diameter of 40 mm (λ_{temp} = 1.8) (Figure 4a-b1) and then immediately released. The duration of time to fully inflate and then deflate the balloon was ~1 minute, excluding intermittent breaks to refill the syringe and monitor the diameter of inflation. After 24 hours, the devices had recovered to new permanent diameters of 23.26 ± 0.38 mm (mean ± s.d.) (λ_{perm} = 1.06 ± 0.02) (Figure 4c1). A second dilation was performed to a maximum diameter of 44 mm (λ_{temp} = 2) (Figure 4b2). During this second dilation, two of the devices, Device #3 and Device #4, sustained tears in their leaflets. The two surviving devices, Device #1 and Device #2, recovered after the second dilation to new permanent diameters of 24.38 ± 0.19 mm (λ_{temp} = 1.11 ± 0.01) (Figure 4c2), showing a greater amount of permanent stretch compared to the uniaxial tests of Elast-Eon™ (λ_{temp} = 2 and λ_{perm} = 1.06 ± 0.03).

Hydrodynamic testing of the four devices under adolescent/adult pulmonary conditions showed good valve function in the pre-dilated state, with effective orifice area (EOA), mean positive pressure differential (PPD), and regurgitant fraction (RF) all at acceptable levels. Device #1 had the thickest leaflets and the highest mean PPD among the four prototypes.

Valve competence was maintained after the first balloon dilation, with increased EOA and decreased mean PPD for all four devices (Table 1). After the second dilation, the two surviving devices both showed additional increases in EOA and decreases in mean PPD. While there are no standard performance requirements for valved prostheses in the pulmonic position, the minimum ISO 5840-2 requirements for EOA in the aortic position were exceeded by nearly all the devices before and after the balloon dilations, except for Device #1 just before and after the first dilation.[55] RF increased after each balloon dilation, but it was maintained well below the maximum of 10% per the ISO 5840–2 requirements for aortic valves. Readings from the pulse duplicator (Figure 5a-e) showed oscillations in flow and ventricular pressure during the valve closing phase. Smaller oscillations in arterial pressure also occurred during valve opening and coincided with visible leaflet flutter (Video S1). The magnitude and frequency of these oscillations generally decreased after each successive balloon dilation.

The effect of the balloon dilation on the valve coaptation height was investigated experimentally. We had modified the original leaflet design of Mackay et al.[54] to have an increased coaptation height h, as defined in Equation (1), in the pre-dilation state. Here, h' is defined as the corresponding dimension (i.e. the remainder of the increased coaptation height) in the post-dilation state. Figure 6 schematically shows valved conduits in the pre-dilation state and after recovering from the first balloon dilation, subjected to fluid pressures of 3 mmHg and 25 mmHg from the distal end to induce valve closure. At a pressure of 3 mmHg, the observed increased coaptation height in the pre-dilation valves was $h_3 = 2.64 \pm 0.34$ mm (mean ± s.d.). The increased coaptation height was smaller in the post-dilation valves, with $h'_3 = 2.11 \pm 0.48$ mm. The same trend was observed at a pressure of 25 mmHg, with $h_{25} = 2.17 \pm 0.12$ mm and $h'_{25} = 1.83 \pm 0.32$ mm.

2.5 Computational Modeling of the Balloon Dilation

A 22 mm valved conduit finite element model was temporarily dilated to a maximum diameter of 44 mm to mimic the balloon dilation experiment (Video S1). The resulting distribution of permanent deformation was non-uniform in the valve region, with the magnitude of deformation being greatest along the leaflet attachment areas (Figure 7). Since the final expanded geometry of the model was irregular and not cylindrical, a final diameter of 24.9 ± 1.0 mm (mean ± s.d.) was calculated from the mean value of the conduit circumference in the valve region (i.e. the section of conduit encompassing the height of the leaflets). This numerical prediction of permanent stretch ($\lambda_{temp} = 2$ and $\lambda_{perm} = 1.13 \pm 0.05$) showed good agreement with the experimental balloon dilations of the valved conduits ($\lambda_{temp} = 2$ and $\lambda_{perm} = 1.11 \pm 0.01$), but was greater than the results from uniaxial testing of Elast-Eon™ ($\lambda_{temp} = 2$ and $\lambda_{perm} = 1.06 \pm 0.03$).

3 Discussion

Our ultimate goal is to develop an integrated valve and conduit device that can be expanded from 12 mm (neonatal size) to 24 mm (adult size) in diameter using multiple incremental balloon dilations. These Elast-Eon™-based prototypes represent the first proof of concept of an expandable valved conduit with balloon dilations from 22 mm (adolescent size) to over 23 mm in diameter. Additionally, we demonstrated the feasibility of subsequent dilations to reach a diameter over 24 mm, which holds clinical significance since the total expansion from 22 mm to 24 mm would potentially eliminate one reoperation to upsize a valved prosthesis while accommodating an adolescent into adulthood. The tearing observed in two of the devices during their second dilations is likely due to limitations from our manual fabrication process and could be resolved through manufacturing process improvements or with the future development of new biomaterials. *In vitro* testing of the fabricated devices showed excellent valve performance both pre- and post-dilation, with EOA increasing after each successful dilation. The computational model of the device expansion demonstrated good agreement with the experimental dilations while predicting a non-uniform valve expansion which must be considered in future designs.

3.1 Materials Characterization and Selection

While Elast-Eon™ generally exhibited elastomeric behavior, the mechanical tests also showed that it can be permanently stretched, a property that may be used to accommodate patient growth. The resulting permanent stretches were governed by the magnitudes of the temporary stretches and could be reliably reproduced to facilitate predictable growth. The actual amounts of permanent stretch in Elast-Eon™ were small, yet they were still sufficient to demonstrate a proof of concept of growth accommodation. Elast-Eon™ also demonstrated excellent biocompatibility and biostability in a rat subcutaneous model, even after stretching. This critical result suggests that the permanent balloon dilations would not cause the device's biological properties to substantially degrade.

Ultimately, neither Elast-Eon™ nor Carbothane™ is an adequate material for achieving the desired permanent 2x expansion that would be needed long-term to expand a neonatal size device to the adult size. Temporary 2x stretches, which approach the limit of clinical

feasibility, resulted in no greater than a 1.06x permanent stretch for either material during mechanical testing. Meanwhile, excessively large 5x temporary stretches, which are clinically infeasible, resulted in no greater than a ~1.5x permanent stretch. A biomaterial with a greater capacity for permanent, or plastic, deformation would be more desirable for this growth-accommodating device and is an opportunity for future polymer development.

3.2 First-Generation Design

The valve was designed with an increased coaptation area to ensure competence at expanded diameters. This increased area was achieved by increasing the leaflets' radial length and free edge length. Clinically, our experience with the Ozaki technique[56,57] for aortic valve reconstruction in children has shown that a valve designed with increased radial and free edge lengths is compatible with patient growth. However, in the Ozaki design, the increased free edge length is obtained by increasing the width of the entire leaflet. This forces the leaflets, which are cut from a sheet of autologous pericardium, to initially adopt a redundant sinusoidal curvature along the free edge. A dip-molded polymeric valve with such a sinusoidal curvature would likely have poor hydrodynamic function. By fabricating the valve via dip molding, the polymer microstructure is set to remember the geometry of the mold. If the polymeric leaflets were sinusoidally shaped, they would tend to keep their sinusoidal curvature under loading and consequently have decreased mobility and increased resistance during valve opening. Furthermore, as the valve diameter was increased, the sinusoidal leaflets would be forced to unfold and flatten, resulting in higher internal leaflet stresses and reduced durability. We avoided these potential drawbacks by lengthening the leaflets in the radial direction alone and creating a triangular profile to increase the free edge length (Figure 2b), while still obtaining a sufficiently increased coaptation area in the dip-molded valve.

When the valved conduits in this study were expanded, the valve leaflets likely sustained some permanent circumferential stretching that assisted in achieving valve closure at the larger diameter. However, when determining the increased coaptation height and new free edge length required to cover the new lumen area, this circumferential stretching was excluded from the calculations. Also excluded was the potential leaflet elongation that could occur due to extended cycling (i.e. creep) under physiological conditions.[58,59]

A trileaflet design was chosen to mimic the three leaflets of a native pulmonary valve and to maintain the associated physiological flow patterns.[60,61] Trileaflet polymeric valves have shown excellent hemodynamic function and durability.[38,45,52,53] In particular, we selected the ellipto-hyperbolic trileaflet geometry since previous valves with this design sustained over 500 million cycles (equivalent to ~13 years) during *in vitro* fatigue testing.[54] However, future work will also explore bileaflet valve designs, motivated by good clinical outcomes from bileaflet polymeric valve implantation for RVOT repair.[50,62-64] Additionally, Hofferberth et al. demonstrated excellent growth potential and valvular performance with a bileaflet venous valve geometry.[33,65]

3.3 Fabrication

Dip molding is known to be a complex process due to the continuous flow of the liquid polymer and the many parameters that must be controlled, including polymer viscosity, dipping speed, and drying position and temperature.[66] Our manual dip molding process resulted in valved conduits with some variability in conduit wall and leaflet thicknesses (Figure 3). This variability was due to the downward flow of liquid Elast-Eon™ solution along the valved conduit mold, as it was held upright to avoid flow of excess liquid polymer into the void between the two mold halves during the dipping and drying processes. Nevertheless, the conduit thickness variations had little effect on the uniformity of the balloon dilations, as all the devices were expanded to similar permanent diameters (Table 1). The resulting range of leaflet thicknesses was comparable to the dip-molded polyurethane valves of Mackay et al.[54] which reached over 500 million cycles in accelerated wear testing and to drop-coated PCU valves which reached 1 billion cycles.[67]

However, further optimization of the fabrication process is desired, as control of leaflet and conduit wall thickness and uniformity are imperative to long-term hydrodynamic performance and durability.[68,69] Leaflet non-uniformity and insufficient leaflet thickness may also have contributed to the tearing of Devices #3 and #4 upon the second set of balloon dilations. Manufacturing process improvements could include robotic mechanisms for controlling the dipping speed and for tumbling the mold while drying to improve uniformity of polymer distribution,[70,71] as well as spray coating.[72]

3.4 *In Vitro* Evaluation

Four valved conduit prototypes were permanently balloon-expanded from a diameter of 22 mm to 23.26 ± 0.38 mm, and two of the prototypes were further expanded to 24.38 ± 0.19 mm. The devices demonstrated increased EOA, lowered mean PPD, and acceptable increases in RF after each successful balloon dilation when tested under pulmonary conditions (Table 1). These results show the feasibility of balloon expansion of a polymeric valved conduit while preserving valve competence.

The pulse duplicator experiments also highlight the importance of considering valve performance across all stages of growth. As previously noted, there was visible fluttering of the leaflets which appeared to correspond to arterial pressure oscillations during valve opening (Video S1, Figure 5a-e). Flutter is undesirable as it is associated with increased leaflet strains, potentially leading to structural failure and decreased valve durability.[69,73] In the present case, flutter may be explained by the presence of redundant leaflet material associated with the increased coaptation height. Interestingly, the magnitudes of the pressure oscillations were noticeably reduced after each balloon dilation (Figure 5), which suggests that the redundant material became more effectively utilized at the larger diameters and the flutter was possibly reduced. This explanation is also consistent with the observed decreases in coaptation height from the pre-dilation to post-dilation states (Table 1).

While previous valves constructed from Elast-Eon™ variants have already demonstrated good thrombogenic properties in a sheep model,[44] we will further assess device thrombogenicity due to valvular dynamics and shear forces in fluid-structure interaction

(FSI) simulations. These simulations will also explore methods to reduce leaflet flutter and the flow and pressure oscillations observed *in vitro*, since such flow disturbances are known to precipitate thrombosis.[74] Approaches to reduce leaflet flutter include increasing the leaflet thickness[69,75] as well as varying the leaflet material and density. Any such changes would need to be balanced with overall valve performance – as seen in Figure 3d, thicker leaflets can lead to increased mean PPD and decreased EOA. We are also investigating new growth-accommodating valve designs that do not require redundant leaflet material and can thus function more optimally and with improved durability at each stage of growth.

3.5 Computational Modeling of the Balloon Dilation

The finite element analysis of the balloon dilation predicted a final diameter in very good agreement with the experimental dilations. This result highlights the reliability and consistency of the balloon dilations and supports the eventual translation of balloon dilatable materials to the clinic. Interestingly, the model also predicted an inhomogeneous distribution of permanent deformation in the device after expansion (Figure 7). The greatest deformation occurred along the leaflet attachment areas, which contain stress concentrations that lead to higher strains and greater permanent stretching. The appearance of stress concentrations in the complex valved conduit geometry could explain why both the experimental balloon dilations ($\lambda_{perm} = 1.11 \pm 0.01$) and numerical simulation ($\lambda_{perm} = 1.13 \pm 0.05$) of the valved conduits showed greater stretching than in the uniaxial test strips ($\lambda_{perm} = 1.06 \pm 0.03$), which had a simple rectangular geometry. These modeling results also suggest that large dilations could result in tearing along those high-stress regions, which was observed in Devices #3 and #4 during their second balloon dilations. Another implication of the non-uniform deformation predicted by the model is that the pre-dilation and post-dilation devices would not be geometrically similar, further emphasizing the need to consider valve design for all stages of growth.

3.6 Limitations

The mechanical tests and the balloon dilation procedure were conducted in room air at ~25 °C. It is possible that a blood or saline environment at 37 °C would affect the polymers' mechanical response and the resulting permanent stretch. Also, only the central valve region of the conduit was dilated. The proximal and distal ends remained at 22 mm and were not dilated due to the fixed 22 mm size of the pulse duplicator testing fixture. This may have impaired the hydrodynamic performance of the dilated devices. Additionally, the fatigue life of this device has not been tested as we only intended this design to be a proof of concept for an expandable valved conduit.

While rat subcutaneous implantation is an accepted model for initial biocompatibility testing of valve components,[47,76,77] the valved conduit material should ultimately be exposed to circulation and cyclic loading in the valve position of a large animal model to assess not only biocompatibility, but also potential effects on mechanical properties, expandability, and long-term durability. Additionally, the potential for expansion after formation of surgical adhesions around the conduit must be confirmed. Although the impacts of these *in vivo* interactions are unknown, our clinical experience with balloon dilation and stenting in non-valved vascular locations is encouraging, as we know that some permanent deformation

of Gore-Tex® grafts, patched vessels, or previously implanted stents can be achieved at different time points after the initial surgery.

3.7 Outlook

Since the completion of this study, we have identified another biostable material capable of greater than 2x permanent stretch, and we are currently developing a 2nd generation prototype. Based on the results presented here, it is expected that the design of this new prototype will benefit from the optimization of hemodynamics across all stages of growth. To achieve this, we are developing computational simulations of valve kinematics and hemodynamics that will enable the study of various growth-accommodating valve geometries with different numbers of leaflets (e.g. bileaflet vs. trileaflet) and different leaflet heights, widths, and free edge lengths. These simulations will take place within a framework that incorporates the nonlinear FSI physics via coupled finite element and computational fluid dynamics analyses, while also accounting for potentially altered material properties post-dilation. The intent is then to manufacture optimized prototypes, demonstrate their *in vivo* performance and expandability in a large animal model of RVOT replacement in sheep, and with FDA approval, conduct a phase I clinical trial to evaluate their safety for implantation in humans.

The concept of tissue engineering represents the ultimate solution for pediatric heart valves, as the intended result is an autologous organ that will grow and adapt to changes in the patient's physiology.[78,79] The classical methodology for tissue engineering utilizes a biodegradable valve-shaped scaffold that is seeded with cells, matured *in vitro* in a bioreactor, and then implanted in the patient so that leaflet tissue can grow naturally.[80] However, key challenges of this method include maintaining the balance of scaffold biodegradation with extracellular matrix formation, as well as preventing leaflet shortening arising from the contractile nature of seeded cells.[81,82] Novel regenerative techniques, such as those based on in-body tissue architecture[83] or implantation of decellularized scaffolds,[84] have shown up to 1 year of good valve function *in vivo*. However, their long-term growth and durability has yet to be demonstrated.

In contrast, the concept of growth accommodation via balloon dilation of a polymeric valve is based on technologies with greater acceptance in current clinical practice. Catheter-based interventions already represent the standard of care for treating valvular disease, such as with balloon valvuloplasty for valve stenosis[85,86] and post-implantation balloon dilation of transcatheter valves.[87] Biostable polymeric valves have also been successfully translated to the clinic – ePTFE valves are commonly assembled in the operating room and then implanted with excellent results.[50-53] Polyurethane valves manufactured by robotic dip molding (Foldax, Inc., Salt Lake City, Utah) are currently undergoing clinical trials,[88,89] as is the aforementioned Autus Valve.[33,34] Furthermore, tissue-engineered valves currently require months of preparation, while synthetic polymeric devices can be manufactured and mass-produced more quickly. Hence, as tissue-engineering technology continues to mature, balloon-expandable polymeric valves constitute a more realistic near-term solution for pediatric patients and warrant greater attention.

4 Conclusions

In this paper, we have established the first proof of concept of a polymeric valved conduit that can be expanded via transcatheter balloon dilation while maintaining its valvular competence. Four 22 mm diameter valved conduits were balloon dilated to new permanent diameters of 23.26 ± 0.38 mm. Further dilation caused two of the valved conduits to sustain leaflet tears, while the two surviving devices reached final diameters of 24.38 ± 0.19 mm. The expansions in diameter were achieved via permanent deformation of the Elast-Eon™ material, while valve performance at the expanded diameters was maintained using a leaflet design with increased coaptation area. Our results have demonstrated the feasibility of this concept and provide motivation for further development of a polymeric valved conduit that can accommodate the growth of children from a neonate to adult size and reduce the need for multiple open-heart surgeries.

5 Experimental Methods

Mechanical Testing:

We evaluated the mechanical behavior of two commercially available, biostable and biocompatible polymers: Carbothane™ AC-4075A (Lubrizol, Cleveland, Ohio) and Elast-Eon™ E5-325 (Biomerics, Salt Lake City, Utah). To prepare material samples, pellets of either Carbothane™ (20% w/v) or Elast-Eon™ (40% w/v) were dissolved in N,N-Dimethylacetamide (99.5%, ACROS Organics, Fair Lawn, New Jersey) to create a viscous solution. After the dissipation of bubbles (~24 hours), the polymer solution was cast onto flat plates and then dried in an oven for 1 hour at 80 °C and ambient pressure. The resulting polymer films were cut into individual specimens for testing, and the thicknesses of the specimens were measured using a digital thickness gauge (Mitutoyo 547-526S, Mitutoyo Corporation, Tokyo, Japan).

All mechanical tests were performed in air at ambient temperature (~25 °C) using an Instron MicroTester 5848 with a 50 N load cell (Instron, Norwood, Massachusetts), and all measurements were taken from distinct samples. Sample strain was measured using the machine crosshead displacement. To obtain the elongations at break and ultimate strengths, dog-bone samples with a 22 mm gauge length were cut with an American Society for Testing and Materials (ASTM) D1708 cutting die (Ace Steel Rule Dies, Medford, New Jersey). The samples were then uniaxially stretched at a strain rate of 0.0067 s^{-1} to match the strain rate used for the stretch tests.

For the stress relaxation tests, 1x4 cm rectangular samples were individually mounted with a 15 mm gauge length between the Instron machine grips. Each sample was first preconditioned for 5 cycles of stretching to $\lambda = 1.5$ and unloading at a strain rate of 0.1 s^{-1}. Then, it was stretched again at the same strain rate and held at a constant stretch of $\lambda = 1.5$ for 300 seconds while the load on the sample was monitored.

For the stretch tests, 1x4 cm rectangular samples were individually mounted with a 15 mm gauge length between the Instron machine grips and then uniaxially stretched to a single predetermined stretch ratio ($\lambda = 2$, 3, 4, or 5) at a strain rate of 0.0067 s^{-1} (corresponding to

a machine crosshead speed of 0.1 mm/s). The samples were then immediately released from this stretch by returning the machine grips to the 15 mm gauge length at the same strain rate, with the sample still held in the grips. The amount of immediately recoverable deformation was denoted by the point of return to zero stress. The samples were then removed from the machine grips and allowed to recover viscoelastically with no external loading. Prior to the start of the test, the gauge length between the grip edges was also marked with a marker. After removal from the testing machine, the amount of strain in each sample was tracked by measuring the distance between these marks. The final permanent stretch was measured 24 hours after the end of each test.

In Vivo Biocompatibility Testing:

8 mm disc specimens were subcutaneously implanted[47,48,76] in 4-month-old male Sprague-Dawley rats (n = 3; Charles River Laboratories, Wilmington, Massachusetts) for a period of two months. Each animal received four specimens, with one specimen made from each polymer. Upon explantation, the material specimens were harvested, sectioned, and stained with hematoxylin and eosin (H&E) and Alizarin Red.

The experimental animal protocol was approved by the Columbia University Institutional Animal Care and Use Committee (IACUC #AC-AABD5614). Animals received humane care in accordance with the “Guide for the Care and Use of Laboratory Animals” (National Research Council, Eight Edition, 2011). These animal experiments did not use a method of randomization, and the investigators were not blinded to allocation during data collection and analysis.

Animals were housed in the Black Building on the campus of the Columbia University Irving Medical Center and treated under the supervision of the Columbia University Institute of Comparative Medicine (ICM). The rats were not subjected to water or food restrictions. ICM animal care staff conducted routine husbandry procedures (cage cleaning, feeding and watering). Full time ICM veterinarian staff monitored the rats at least twice a day to assess their condition. The veterinary staff was available at all times and assisted with surgical procedures, injections and sample harvesting.

Rats were initially anesthetized with isofluorane inhalation (4%) via an induction chamber and then maintained with isoflurane at 1.0-1.5% via nose cone during the polymer patch implantation. After implantation, the rats were allowed to recover on a warm pad at 37 °C and returned to the cage once awake. Potential pain was assessed every 2 days and relieved by Meloxicam administration. If any of the following sign/symptoms were noted analgesic was administered: decreased activity, hunched posture, lack of grooming, abnormal gait. Lack of appetite or water consumption was noted.

Rats were euthanized by isoflurane overdose, a method consistent with the recommendations of the Panel on Euthanasia of the American Veterinary Medical Association. Death was verified by cervical dislocation since the IACUC approves this method as quick and painless on small animals.

Fabrication by Dip Molding:

The device prototypes were formed by dip molding. First, the geometry of the valved conduit was modeled in the computer-aided design (CAD) program SolidWorks (Dassault Systèmes, Waltham, Massachusetts) and used to design a two-piece mold, which was then machined in aluminum by 5-axis computer numerical control (CNC) milling (Protolabs, Maple Plain, Minnesota). To form the leaflets, the positive end of the mold was manually dipped into a liquid solution of Elast-Eon™ (40% w/v in N,N-Dimethylacetamide) and then dried in an oven at 80 °C for >12 hours, evaporating the solvent and leaving a conformal polymer coating. Next, the negative end of the mold was fitted over the positive end with the first coating still intact, and the fully assembled mold was dipped and then dried to form the conduit. Conduit thickness was increased using additional rounds of dipping and drying – 4 rounds total for all devices. After the final round, the polymer-coated mold was removed from the oven, cooled to room temperature, and then soaked in water for 15 minutes to loosen the polymer from the mold. Finally, the polymer was carefully peeled from the mold, and the three leaflets were separated using a sharp blade.

Conduit wall thickness was measured pre-dilation using a digital thickness gauge (Mitutoyo 547-526S, Mitutoyo Corporation, Tokyo, Japan) at locations proximal to the valve, distal to the valve, and in the middle of the conduit just slightly distal to the valve. At each of the three locations, three measurements were taken at equidistant sites along the circumference of the conduit. After the completion of *in vitro* device evaluation involving dilation as detailed below, the leaflets were excised from the conduit, and their thicknesses were mapped. The thickness of each leaflet was measured at four different sites spanning the top, middle, and bottom of the leaflet.

In Vitro Evaluation:

Permanent dilation of the valved conduits was performed using a 46 mm diameter Coda balloon catheter (Cook Medical, Bloomington, Indiana). The balloon was filled using a syringe to the target diameters. The balloon was inflated to a 40 mm diameter, using a 40 mm inner diameter 3D-printed ring as an indicator, and then immediately released with no holding time. The new permanent diameters of the valved conduits were measured 24 hours after the balloon dilations. The second round of balloon dilations was performed in a similar manner, but to a diameter of 44 mm.

The *in vitro* hydrodynamic function of the prototypes was evaluated before and after the balloon dilations using a commercial heart valve pulse duplicator (HDTi 6000, BDC Laboratories, Wheat Ridge, Colorado) equipped with a flow meter (Transonic Systems, Ithaca, New York) and upstream and downstream pressure transducers (BDC Laboratories). The devices were tested using pulmonary conditions at 15 mmHg mean arterial pressure (70 bpm heart rate, 70 mL stroke volume, systole comprising 35% of the cardiac cycle, and a working fluid of 1% w/v saline solution).

Regurgitant fraction (RF), mean positive pressure differential (PPD), and effective orifice area (EOA) were calculated using Statys™ software (BDC Laboratories) in accordance with ISO 5840-1:2021, and the results were averaged over ten consecutive cardiac cycles.

The mean PPD, where pressure differential (PD) is defined by

$$\mathrm{PD} = ventricular\ pressure - arterial\ pressure, \tag{2}$$

was calculated over the time period ranging from the start of the positive pressure differential ($ventricular\ pressure > arterial\ pressure$) to the end of the positive pressure differential. The effective orifice area was calculated as

$$\mathrm{EOA} = \frac{q_{vRMS}}{51.6 \times \sqrt{\frac{\Delta p}{\rho}}}, \tag{3}$$

where q_{vRMS} is the root mean square forward flow (ml/s) during the positive differential pressure period, Δp is the mean PPD (mmHg) during the same period, and ρ is the density of the test fluid (g·cm^{-3}). The regurgitant fraction was calculated as

$$\mathrm{RF} = \frac{Closing\ volume + Leakage\ volume}{Forward\ flow\ volume}. \tag{4}$$

We measured the coaptation heights of each valved conduit before and after the balloon dilations. The prototypes were first mounted vertically in a test fixture (BDC Laboratories) with the distal end facing upwards and a 25.4 mm inner diameter clear polycarbonate tube affixed to the top of the test fixture. Then, tap water at ~25 °C was poured into the distal end of the tube to generate pressure heads corresponding to pressures of 3 mmHg, which was just sufficient to close the valves, and 25 mmHg, which is the typical peak diastolic pressure in the pulmonary artery. The pressure was monitored using a pressure transducer (BDC Laboratories) and Statys™ software (BDC Laboratories). Images of the valves in the closed states were recorded with a digital camera, and measurements were taken using ImageJ software (National Institutes of Health, Bethesda, Maryland). The recorded coaptation height was averaged from three measurements.

Computational Modeling of the Balloon Dilation:

The expansion of the valved conduit was simulated using a mechanical finite element analysis (FEA) model (Abaqus, Dassault Systèmes) with a calibrated Elast-Eon™ material model. The FEA model was constructed from the geometry of the valve using shell elements. A uniform thickness of 100 μm was assigned throughout the structure to match the measured thicknesses of the leaflets. The balloon was modeled as a rigid cylindrical structure using membrane elements that were rigidly constrained, and the dilation was simulated via a uniform radial expansion. The nonlinear elastic material response in the valved conduit was modeled using an Ogden-type hyperelastic model.[90] The permanent, inelastic deformation was approximated by a J_2-plasticity model,[91,92] while Mullins effect was captured using a damage model.[93,94] Material calibration and construction of the FEA model are further described in the Supporting Information section.

Statistical Analyses:

Results were analyzed using OriginPro 2016 (OriginLab, Northampton, Massachusetts). Mechanical and hydrodynamic data and device thicknesses are expressed as mean ± standard deviation. Device diameters and coaptation heights are expressed as the measurement ± estimated measurement error. Mechanical data and thickness measurements were analyzed for statistical significance by the unpaired Student's t-test (two-sided), with $p < 0.05$ considered statistically significant.

Supplementary Material

Refer to Web version on PubMed Central for supplementary material.

Acknowledgements

The authors would like to thank Dr. Yingfei Xue, Dr. Antonio Frasca, and Kenneth Cai for helpful discussions and for their assistance with *in vitro* and *in vivo* testing. The authors would also like to thank Andrew Weiss and Ernesto Cabello of Piper Plastics Corp. for their technical guidance on dip molding.

This work was supported by the National Institutes of Health, Bethesda, Maryland [R01-HL-155381] (DK), [R01-HL-143008] (GF), [T32-HL007854] (APK); the Thoracic Surgery Foundation Research Award, Chicago, Illinois (DK); the Kibel Fund for Aortic Valve Research, Philadelphia, Pennsylvania (GF); the Congenital Heart Defect Coalition, Butler, New Jersey (DK); the Babies Heart Fund for Research in Congenital Heart Disease, New York, New York (DK); the Columbia University Provost Seed Grant, New York, New York (DK); the Columbia University Alliance Joint Projects Grant, New York, New York (DK); the Columbia Irving Scholar Award, New York, New York (DK); the Post-9/11 G.I. Bill (RLL); the Columbia University Yellow Ribbon Program, New York, New York (RLL); and the National Science Foundation Graduate Research Fellowship under Grant No. DGE-2036197 (ARH).

Data Availability Statement

The data that support the findings of this study are available from the corresponding author upon reasonable request.

References

[1]. van der Linde D, Konings EEM, Slager MA, Witsenburg M, Helbing WA, Takkenberg JJM, Roos-Hesselink JW, J. Am. Coll. Cardiol 2011, 58, 2241. [PubMed: 22078432]

[2]. Roger VL, Go AS, Lloyd-Jones DM, Adams RJ, Berry JD, Brown TM, Carnethon MR, Dai S, de Simone G, Ford ES, Fox CS, Fullerton HJ, Gillespie C, Greenlund KJ, Hailpern SM, Heit JA, Ho PM, Howard VJ, Kissela BM, Kittner SJ, Lackland DT, Lichtman JH, Lisabeth LD, Makuc DM, Marcus GM, Marelli A, Matchar DB, McDermott MM, Meigs JB, Moy CS, Mozaffarian D, Mussolino ME, Nichol G, Paynter NP, Rosamond WD, Sorlie PD, Stafford RS, Turan TN, Turner MB, Wong ND, Wylie-Rosett J, Circulation 2011, 123, 18.

[3]. Hoffman JIE, Kaplan S, J. Am. Coll. Cardiol 2002, 39, 1890. [PubMed: 12084585]

[4]. Reller MD, Strickland MJ, Riehle-Colarusso T, Mahle WT, Correa A, J. Pediatr 2008, 153, 807. [PubMed: 18657826]

[5]. Kaza AK, Lim HG, Dibardino DJ, Bautista-Hernandez V, Robinson J, Allan C, Laussen P, Fynn-Thompson F, Bacha E, del Nido PJ, Mayer JE, Pigula FA, J. Thorac. Cardiovasc. Surg 2009, 138, 911. [PubMed: 19660342]

[6]. Karamlou T, Jang K, Williams WG, Caldarone CA, Van Arsdell G, Coles JG, McCrindle BW, Circulation 2005, 112, 3462. [PubMed: 16316968]

[7]. Dvir D, Bourguignon T, Otto CM, Hahn RT, Rosenhek R, Webb JG, Treede H, Sarano ME, Feldman T, Wijeysundera HC, Topilsky Y, Aupart M, Reardon MJ, Mackensen GB, Szeto WY, Kornowski R, Gammie JS, Yoganathan AP, Arbel Y, Borger MA, Simonato M, Reisman M,

Makkar RR, Abizaid A, McCabe JM, Dahle G, Aldea GS, Leipsic J, Pibarot P, Moat NE, Mack MJ, Kappetein AP, Leon MB, Circulation 2018, 137, 388. [PubMed: 29358344]

[8]. David TE, Armstrong S, Maganti M, Ann. Thorac. Surg 2010, 90, 775. [PubMed: 20732495]

[9]. Bourguignon T, Bouquiaux-Stablo AL, Candolfi P, Mirza A, Loardi C, May MA, El-Khoury R, Marchand M, Aupart M, Ann. Thorac. Surg 2015, 99, 831. [PubMed: 25583467]

[10]. Neves JP, Gulbenkian S, Ramos T, Martins AP, Caldas MC, Mascarenhas R, Guerreiroa M, Matoso-Ferreira A, Santos R, Monteiro C, Melo JQ, J. Thorac. Cardiovasc. Surg 1997, 113, 1014. [PubMed: 9202681]

[11]. Kanter KR, Kirshbom PM, Kogon BE, Ann. Thorac. Surg 2006, 82, 1594. [PubMed: 17062211]

[12]. Iung B, Rodes-Cabau J, Eur. Heart J 2014, 35, 2942. [PubMed: 25205532]

[13]. Nomoto R, Sleeper LA, Borisuk MJ, Bergerson L, Pigula FA, Emani S, Fynn-Thompson F, Mayer JE, del Nido PJ, Baird CW, J. Thorac. Cardiovasc. Surg 2016, 152, 1333. [PubMed: 27637422]

[14]. Karamlou T, Blackstone EH, Hawkins JA, Jacobs ML, Kanter KR, Brown JW, Mavroudis C, Caldarone CA, Williams WG, McCrindle BW, J. Thorac. Cardiovasc. Surg 2006, 132, 829. [PubMed: 17000294]

[15]. da Costa FDA, Etnel JRG, Charitos EI, Sievers HH, Stierle U, Fornazari D, Takkenberg JJM, Bogers AJJC, Mokhles MM, Ann. Thorac. Surg 2018, 105, 1205. [PubMed: 29307455]

[16]. Belli E, Salihoğlu E, Leobon B, Roubertie F, Ly M, Roussin R, Serraf A, Ann. Thorac. Surg 2010, 89, 152. [PubMed: 20103226]

[17]. Tweddell JS, Pelech AN, Frommelt PC, Mussatto KA, Wyman JD, Fedderly RT, Berger S, Frommelt MA, Lewis DA, Friedberg DZ, Thomas JP, Sachdeva R, Litwin SB, Circulation 2000, 102, DOI 10.1161/circ.102.suppl_3.III-130.

[18]. Chen PC, Sager MS, Zurakowski D, Pigula FA, Baird CW, Mayer JE, del Nido PJ, Emani SM, J. Thorac. Cardiovasc. Surg 2012, 143, 352. [PubMed: 22153723]

[19]. Saleeb SF, Newburger JW, Geva T, Baird CW, Gauvreau K, Padera RF, del Nido PJ, Borisuk MJ, Sanders SP, Mayer JE, Circulation 2014, 130, 51. [PubMed: 24756063]

[20]. Fuller SM, Borisuk MJ, Sleeper LA, Bacha E, Burchill L, Guleserian K, Ilbawi M, Razzouk A, Shinkawa T, Lu M, Baird CW, Semin. Thorac. Cardiovasc. Surg 2021, DOI 10.1053/j.semtcvs.2021.06.020.

[21]. Yamamoto Y, Yamagishi M, Miyazaki T, Gen. Thorac. Cardiovasc. Surg 2015, 63, 131. [PubMed: 25503561]

[22]. Kostyunin AE, Yuzhalin AE, Rezvova MA, Ovcharenko EA, Glushkova TV, Kutikhin AG, J. Am. Heart Assoc 2020, 9, 1.

[23]. Christian AJ, Lin H, Alferiev IS, Connolly JM, Ferrari G, Hazen SL, Ischiropoulos H, Levy RJ, Biomaterials 2014, 35, 2097. [PubMed: 24360721]

[24]. Lee S, Levy RJ, Christian AJ, Hazen SL, Frick NE, Lai EK, Grau JB, Bavaria JE, Ferrari G, J. Am. Heart Assoc 2017, 6, 1.

[25]. Gomel MA, Lee R, Grande-Allen KJ, Front. Cardiovasc. Med 2019, 5, 1.

[26]. Liao KK, Li X, John R, Amatya DM, Joyce LD, Park SJ, Bianco R, Bolman RM, Ann. Thorac. Surg 2008, 86, 491. [PubMed: 18640322]

[27]. Flameng W, Herregods M-C, Vercalsteren M, Herijgers P, Bogaerts K, Meuris B, Circulation 2010, 121, 2123. [PubMed: 20439787]

[28]. Emani SM, Piekarski BL, Zurakowski D, Baird CA, Marshall AC, Lock JE, del Nido PJ, J. Thorac. Cardiovasc. Surg 2016, 152, 1514. [PubMed: 27692768]

[29]. Feins EN, Chávez M, Callahan R, del Nido PJ, Emani SM, Baird CW, Ann. Thorac. Surg 2020, DOI 10.1016/j.athoracsur.2020.05.061.

[30]. Pluchinotta FR, Piekarski BL, Milani V, Kretschmar O, Burch PT, Hakami L, Meyer DB, Jacques F, Ghez O, Trezzi M, Carotti A, Qureshi SA, Michel-Behnke I, Hammel JM, Chai P, McMullan D, Mettler B, Ferrer Q, Carminati M, Emani SM, Circ. Cardiovasc. Interv 2018, 11, 1.

[31]. Sullivan PM, Wong PC, Kim R, Ing FF, Cardiol. Young 2019, 29, 235. [PubMed: 30511601]

[32]. Langer NB, Solowiejczyk D, Fahey JT, Torres A, Bacha E, Kalfa D, J. Thorac. Cardiovasc. Surg 2018, 156, 1190. [PubMed: 29709362]

[33]. Hofferberth SC, Saeed MY, Tomholt L, Fernandes MC, Payne CJ, Price K, Marx GR, Esch JJ, Brown DW, Brown J, Hammer PE, Bianco RW, Weaver JC, Edelman ER, del Nido PJ, Sci. Transl. Med 2020, 12, eaay4006. [PubMed: 32075944]

[34]. "Autus Size-Adjustable Valve for Surgical Pulmonary Valve Replacement Early Feasibility Study," can be found under https://clinicaltrials.gov/ct2/show/NCT05006404, **n.d.n.d.**

[35]. Feins EN, Emani SM, Semin. Thorac. Cardiovasc. Surg. Pediatr. Card. Surg. Annu 2020, 23, 17. [PubMed: 32354541]

[36]. Manavitehrani I, Ebrahimi P, Yang I, Daly S, Schindeler A, Saxena A, Little DG, Fletcher DF, Dehghani F, Winlaw DS, Cardiovasc. Eng. Technol 2019, DOI 10.1007/s13239-019-00406-5.

[37]. Stradins P, Lacis R, Ozolanta I, Purina B, Ose V, Feldmane L, Kasyanov V, Eur. J. Cardio-thoracic Surg 2004, 26, 634.

[38]. Li RL, Russ J, Paschalides C, Ferrari G, Waisman H, Kysar JW, Kalfa D, Biomaterials 2019, 225, 119493. [PubMed: 31569017]

[39]. Bélanger MC, Marois Y, Roy R, Mehri Y, Wagner E, Zhang Z, King MW, Yang M, Hahn C, Guidoin R, Artif. Organs 2000, 24, 879. [PubMed: 11119076]

[40]. Yang M, Zhang Z, Hahn C, Laroche G, King MW, Guidoin R, J. Biomed. Mater. Res 1999, 48, 13. [PubMed: 10029144]

[41]. Yang M, Zhang Z, Hahn C, King MW, Guidoin R, J. Biomed. Mater. Res 1999, 48, 648. [PubMed: 10490678]

[42]. Bernacca GM, Straub I, Wheatley DJ, J. Biomed. Mater. Res 2002, 61, 138. [PubMed: 12001256]

[43]. Simmons A, Hyvarinen J, Odell RA, Martin DJ, Gunatillake PA, Noble KR, Poole-Warren LA, Biomaterials 2004, 25, 4887. [PubMed: 15109849]

[44]. Wheatley DJ, Bernacca GM, Tolland MM, O'Connor B, Fisher J, Williams DF, Int. J. Artif. Organs 2001, 24, 95. [PubMed: 11256515]

[45]. Bezuidenhout D, Williams DF, Zilla P, Biomaterials 2015, 36, 6. [PubMed: 25443788]

[46]. Levy RJ, Schoen FJ, Levy JT, Nelson AC, Howard SL, Oshry LJ, Am. J. Pathol 1983, 113, 143. [PubMed: 6605687]

[47]. Bonetti A, Marchini M, Ortolani F, J. Thorac. Dis 2019, 11, 2126. [PubMed: 31285908]

[48]. Frasca A, Xue Y, Kossar AP, Keeney S, Rock C, Zakharchenko A, Streeter M, Gorman RC, Grau JB, George I, Bavaria JE, Krieger A, Spiegel DA, Levy RJ, Ferrari G, JACC Basic to Transl. Sci 2020, 5, 755.

[49]. Christian AJ, Alferiev IS, Connolly JM, Ischiropoulos H, Levy RJ, J. Biomed. Mater. Res. - Part A 2015, 103, 2441.

[50]. Quintessenza JA, Jacobs JP, Chai PJ, Morell VO, Lindberg H, World J. Pediatr. Congenit. Hear. Surg 2010, 1, 20.

[51]. Ando M, Takahashi Y, J. Thorac. Cardiovasc. Surg 2009, 137, 124. [PubMed: 19154914]

[52]. Miyazaki T, Yamagishi M, Maeda Y, Taniguchi S, Fujita S, Hongu H, Yaku H, J. Thorac. Cardiovasc. Surg 2018, 155, 2567. [PubMed: 29510932]

[53]. Yamashita E, Yamagishi M, Miyazaki T, Maeda Y, Yamamoto Y, Kato N, Asada S, Hongu H, Yaku H, Ann. Thorac. Surg 2016, 102, 1336. [PubMed: 27173066]

[54]. Mackay TG, Wheatley DJ, Bernacca GM, Fisher AC, Hindle CS, Biomaterials 1996, 17, 1857. [PubMed: 8889065]

[55]. International Organization for Standardization, Cardiovascular Implants - Cardiac Valve Prostheses - Part 2: Surgically Implanted Heart Valve Substitutes (ISO 5840-2:2021), 2021.

[56]. Ozaki S, Kawase I, Yamashita H, Uchida S, Nozawa Y, Matsuyama T, Takatoh M, Hagiwara S, Interact. Cardiovasc. Thorac. Surg 2011, 12, 550. [PubMed: 21273254]

[57]. Ozaki S, Kawase I, Yamashita H, Uchida S, Takatoh M, Kiyohara N, J. Thorac. Cardiovasc. Surg 2018, 155, 2379. [PubMed: 29567131]

[58]. Bernacca GM, O'Connor B, Williams DF, Wheatley DJ, Biomaterials 2002, 23, 45. [PubMed: 11762853]

[59]. Kidane AG, Burriesci G, Edirisinghe M, Ghanbari H, Acta Biomater. 2009, 5, 2409. [PubMed: 19497802]

[60]. Sotiropoulos F, Le TB, Gilmanov A, Annu. Rev. Fluid Mech 2016, 48, 259.

[61]. Daebritz SH, Fausten B, Hermanns B, Franke A, Schroeder J, Groetzner J, Autschbach R, Messmer BJ, Sachweh JS, Heart Surg. Forum 2004, 7, 371.

[62]. Shinkawa T, Tang X, Gossett JM, Mustafa T, Hategekimana F, Watanabe F, Miyazaki T, Yamagishi M, Imamura M, Ann. Thorac. Surg 2015, 100, 129. [PubMed: 26004923]

[63]. Choi KH, Sung SC, Kim H, Lee HD, Kim G, Ko H, J. Card. Surg 2018, 33, 36. [PubMed: 29314335]

[64]. Lee C, Lee CH, Kwak JG, Song JY, Shim WS, Choi EY, Lee SY, Kim YM, Eur. J. Cardio-thoracic Surg 2013, 43, 468.

[65]. Hammer PE, Roberts EG, Emani SM, del Nido PJ, J. Thorac. Cardiovasc. Surg 2017, 153, 389. [PubMed: 27665220]

[66]. Bezuidenhout D, Williams DF, Zilla P, Biomaterials 2015, 36, 6. [PubMed: 25443788]

[67]. Daebritz SH, Circulation 2003, 108, 134.

[68]. Stasiak J, Serrani M, Biral E, Taylor J, Zaman A, Jones S, Ness T, de Gaetano F, Costantino ML, Bruno VD, Suleiman M-S, Ascione R, Moggridge G, Biomater. Sci 2020, DOI 10.1039/d0bm00412j.

[69]. Johnson EL, Wu MCH, Xu F, Wiese NM, Rajanna MR, Herrema AJ, Ganapathysubramanian B, Hughes TJR, Sacks MS, Hsu M-C, Proc. Natl. Acad. Sci 2020, 117, 19007. [PubMed: 32709744]

[70]. Jansen J, Reul H, J. Med. Eng. Technol 1992, 16, 27. [PubMed: 1640445]

[71]. Rahmani B, Tzamtzis S, Ghanbari H, Burriesci G, Seifalian AM, J. Biomech 2012, 45, 1205. [PubMed: 22336198]

[72]. Park KS, Appa H, Visagie C, Bezuidenhout D, Zilla PP, A Prosthetic Heart Valve, 2016, US 2016/0067038.

[73]. Vennemann B, Rösgen T, Heinisch PP, Obrist D, ASAIO J 2018, 64, 651. [PubMed: 29045279]

[74]. Scotten LN, Siegel R, J. Heart Valve Dis 2011, 20, 664. [PubMed: 22655497]

[75]. Lee JH, Scotten LN, Hunt R, Caranasos TG, Vavalle JP, Griffith BE, JTCVS Open 2021, 6, 60. [PubMed: 35211686]

[76]. Sun M, Elkhodiry M, Shi L, Xue Y, Abyaneh MH, Kossar AP, Giuglaris C, Carter SL, Li RL, Bacha E, Ferrari G, Kysar J, Myers K, Kalfa D, Biomaterials 2022, 288, 121756. [PubMed: 36041938]

[77]. Xue Y, Kossar AP, Abramov A, Frasca A, Sun M, Zyablitskaya M, Paik D, Kalfa D, Della Barbera M, Thiene G, Kozaki S, Kawashima T, Gorman JH III, Gorman RC, Gillespie MJ, Carreon CK, Sanders SP, Levy RJ, Ferrari G, Cardiovasc. Res 2022, cvac002.

[78]. Bouten CVC, Smits AIPM, Baaijens FPT, Front. Cardiovasc. Med 2018, 5, 1. [PubMed: 29404341]

[79]. Boyd R, Parisi F, Kalfa D, Semin. Thorac. Cardiovasc. Surg 2019, 31, 807. [PubMed: 31176798]

[80]. Langer R, Vacanti J, Science (80-.). 1993, 260, 920.

[81]. Driessen-Mol A, Emmert MY, Dijkman PE, Frese L, Sanders B, Weber B, Cesarovic N, Sidler M, Leenders J, Jenni R, Grünenfelder J, Falk V, Baaijens FPT, Hoerstrup SP, J. Am. Coll. Cardiol 2014, 63, 1320. [PubMed: 24361320]

[82]. Weber B, Dijkman PE, Scherman J, Sanders B, Emmert MY, Grünenfelder J, Verbeek R, Bracher M, Black M, Franz T, Kortsmit J, Modregger P, Peter S, Stampanoni M, Robert J, Kehl D, van Doeselaar M, Schweiger M, Brokopp CE, Wälchli T, Falk V, Zilla P, Driessen-Mol A, Baaijens FPT, Hoerstrup SP, Biomaterials 2013, 34, 7269. [PubMed: 23810254]

[83]. Kawashima T, Umeno T, Terazawa T, Wada T, Shuto T, Nishida H, Anai H, Nakayama Y, Miyamoto S, Interact. Cardiovasc. Thorac. Surg 2021, 32, 969. [PubMed: 33543242]

[84]. Syedain ZH, Haynie B, Johnson SL, Lahti M, Berry J, Carney JP, Li J, Hill RC, Hansen KC, Thrivikraman G, Bianco R, Tranquillo RT, Sci. Transl. Med 2021, 13, eabb7225. [PubMed: 33731437]

[85]. Otto CM, Mickel MC, Kennedy JW, Alderman EL, Bashore TM, Block PC, Brinker JA, Diver D, Ferguson J, Holmes DR, Circulation 1994, 89, 642. [PubMed: 8313553]

[86]. Alsawah GA, Hafez MM, Matter M, Abo-Haded HM, Rakha S, Almarsafawy H, Prog. Pediatr. Cardiol 2016, 43, 127.

[87]. Hahn RT, Pibarot P, Webb J, Rodes-Cabau J, Herrmann HC, Williams M, Makkar R, Szeto WY, Main ML, Thourani VH, Tuzcu EM, Kapadia S, Akin J, McAndrew T, Xu K, Leon MB, Kodali SK, JACC Cardiovasc. Interv 2014, 7, 781. [PubMed: 25060022]

[88]. "Early Feasibility Study for the Foldax Tria Aortic Heart Valve," can be found under https://clinicaltrials.gov/ct2/show/NCT03851068, **n.d.n.d.**

[89]. "Early Feasibility Study for the Foldax TRIA Mitral Heart Valve Replacement Investigational Device Exemption," can be found under https://clinicaltrials.gov/ct2/show/NCT04717570, **n.d.n.d.**

[90]. Ogden RW, Proc. R. Soc. London. Ser. A Math. Phys. Sci 1972, 326, 565.

[91]. Simo JC, Comput. Methods Appl. Mech. Eng 1992, 99, 61.

[92]. Weber G, Anand L, Comput. Methods Appl. Mech. Eng 1990, 79, 173.

[93]. Govindarajan SM, Hurtado J, Mars W, in Proc. 5th Eur. Conf. Const. Model. Rubber, ECCMR 2007, Paris, 2008, pp. 249–254.

[94]. ABAQUS User's Manual, Dassault Systèmes Simulia Corp., Providence, RI, 2019.

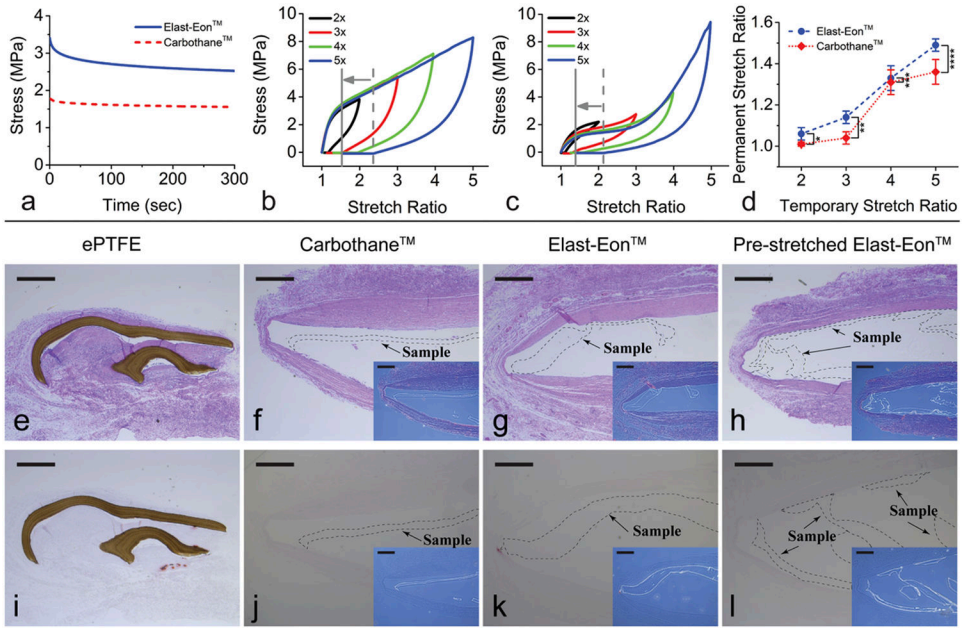

Figure 1. Mechanical characterization and in vivo biocompatibility testing of Elast-EonTM and Carbothane™

(a) The averaged (mean) responses from stress relaxation tests of Elast-Eon™ and Carbothane™ (n = 4 samples per group) show significant dissipation of time-dependent viscous effects within the first 300 seconds of an induced strain. Standard deviation is ± 0.03 MPa for both Elast-Eon™ and Carbothane™. **(b-c)** Representative stress-stretch curves for distinct samples of **(b)** Elast-Eon™ and **(c)** Carbothane™ showing elastomeric mechanical behavior when stretched uniaxially to stretch ratios of λ_{temp} = 2 (black line), λ_{temp} = 3 (red line), λ_{temp} = 4 (green line), and λ_{temp} = 5 (blue line) and then unloaded. The dashed gray line indicates the amount of immediate recovery after stretching to λ_{temp} = 5 and then unloading, and the solid gray line indicates the permanent deformation remaining after 24 hours. **(d)** Amount of permanent stretch resulting from different temporary stretch ratios. Blue circles and red diamonds represent the mean values, and error bars represent the standard deviation. Elast-Eon™ showed greater permanent stretch than Carbothane™ at λ_{temp} = 2, 3, and 5. *p = 0.008; **p = 5e-5; ***p = 0.65 (n.s.); ****p = 0.0038, unpaired Student's t-test (n = 4 to 8 samples per group). **(e-l)** Histological sections stained with hematoxylin and eosin (middle row, e-h) and Alizarin Red (bottom row, i-l) of ePTFE control samples (e, i), non-stretched Carbothane™ (f, j), non-stretched Elast-Eon™ (g, k), and Elast-Eon™ permanently pre-stretched by λ_{perm} = 1.1 (h, l) showing no cell penetration or calcification in a rat subcutaneous model with explantation at 2 months. Insets (f-h, j-l) show the locations of the transparent Carbothane™ and Elast-Eon™ samples. Original magnification 5x; scale bars = 500 μm.

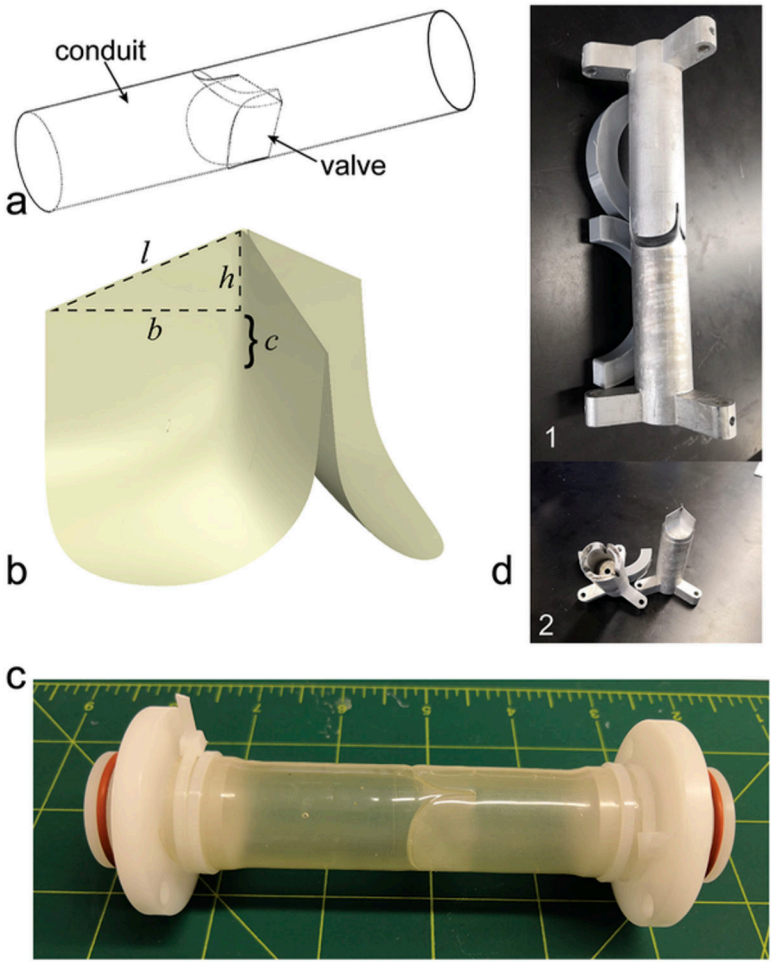

Figure 2. Design and fabrication of the growth-accommodating valved conduit

(a) Design schematic of the growth-accommodating polymeric valved conduit showing a conduit with a trileaflet valve positioned in its center. **(b)** The coaptation area of the original leaflet design by Mackay et al.[54] is characterized by an original coaptation height *c*. We modified this leaflet design to have an increased coaptation area to ensure competence at an expanded valve diameter. This increased area is characterized by an increased coaptation height *h* which forms the side of a right triangle having base length *b* equal to the initial conduit radius and hypotenuse length *l* equal to the expanded conduit radius, as well as a new length of the free edge 2*l* which follows a triangular profile. **(c)** Fabricated valved conduit in the pre-dilation state (22 mm diameter). Grid lines are in inches. **(d1)** Two-piece aluminum mold for dip molding fabrication of Elast-Eon™ valved conduit prototypes. The negative end of the mold is pictured at the top, and the positive end is at the bottom. **(d2)** The two separate pieces of the mold.

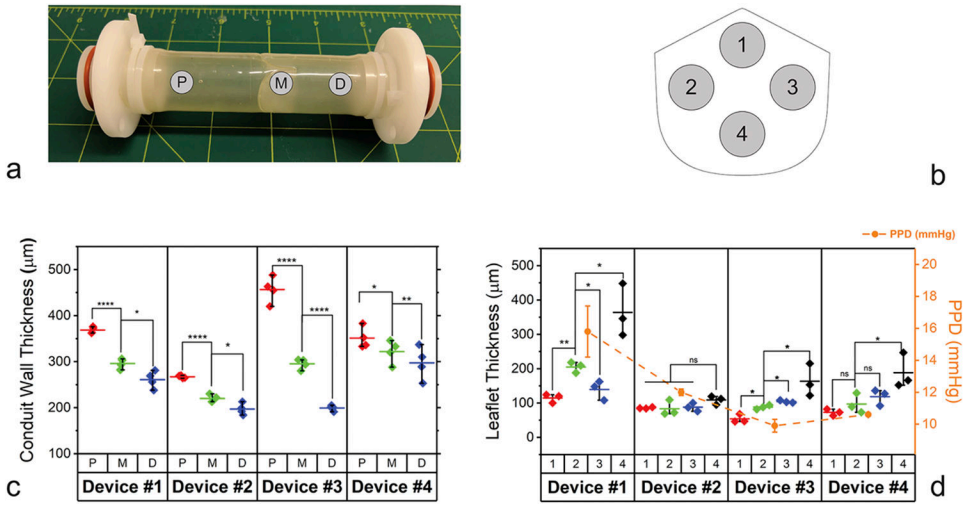

Figure 3. Thicknesses of pre-dilation conduit walls and post-dilation excised leaflets

(a) Conduit wall thickness measurement sites P (proximal), M (middle), and D (distal). **(b)** Leaflet thickness measurement sites 1-4. **(c)** Measurements of pre-dilation conduit wall thickness. **(d)** Measurements of excised, post-dilation leaflet thickness and corresponding mean positive pressure differentials (PPD) from pre-dilation hydrodynamic testing of the valved conduits. For conduit wall and leaflet thicknesses, diamonds represent individual measurements, horizontal bars represent the mean values, and whiskers represent the minimum and maximum values. For mean PPD, circles represent the mean values, and whiskers represent ±1 s.d. *$p < 0.05$, **$p < 0.01$, ****$p < 0.0001$, unpaired Student's t-test ($n = 3$ measurements per group).

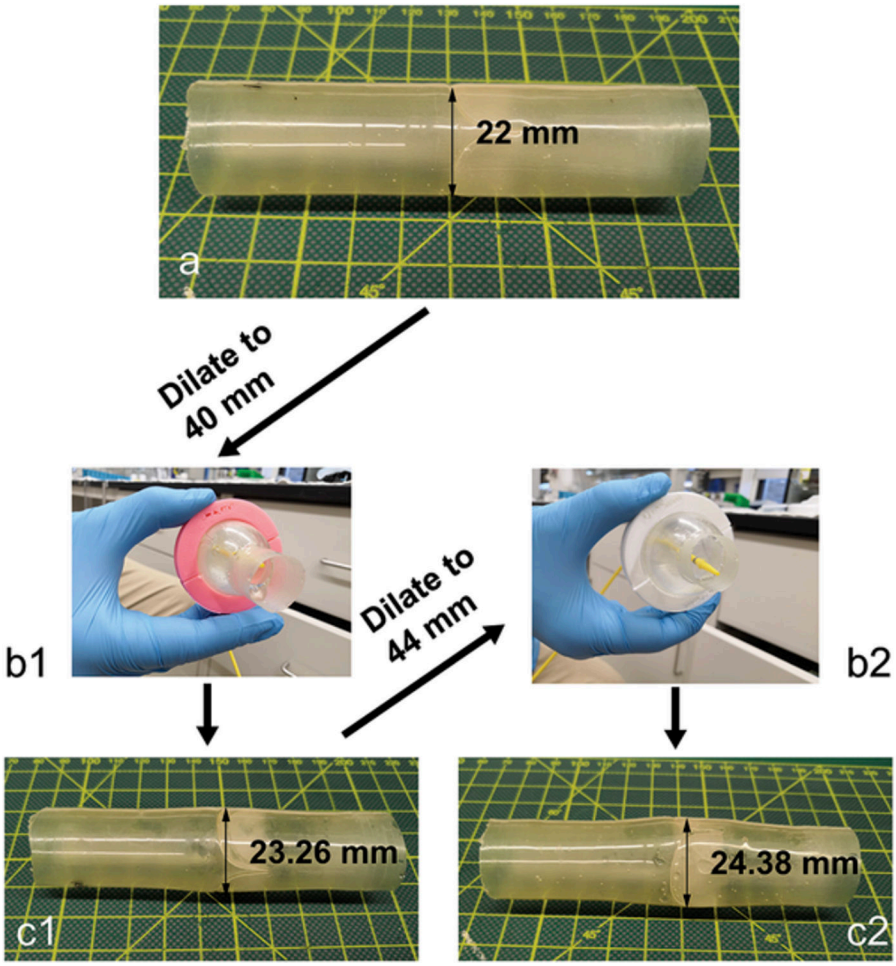

Figure 4. Transcatheter balloon dilation of a valved conduit

Four 22 mm diameter devices **(a)** were temporarily balloon dilated to a diameter of 40 mm using a Coda balloon catheter **(b1)**, after which they recovered to new permanent diameters of 23.26 ± 0.38 mm **(c1)**. The devices were further temporarily dilated to a larger diameter of 44 mm **(b2)** Two of the four devices tore, and the two surviving devices recovered to new permanent diameters of 24.38 ± 0.19 mm **(c2)**.

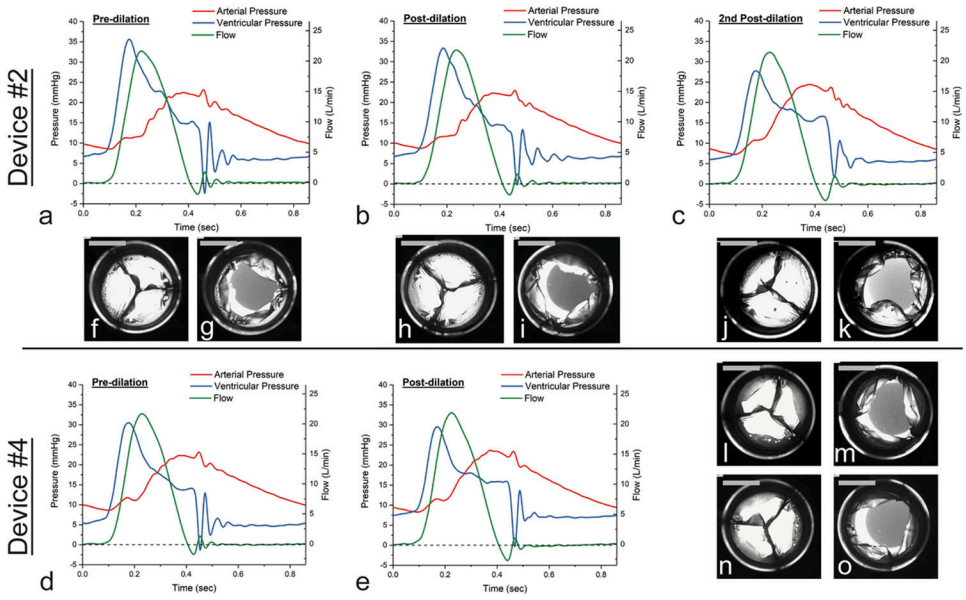

Figure 5. Effects of the balloon dilations on *in vitro* hydrodynamic performance of the valved conduits

(a-e) Representative pulse duplicator readings from a single cardiac cycle for ventricular pressure (blue), arterial pressure (red), and forward flow (green) are shown as a function of time. Pressure and flow oscillations observed in the pre-dilation valves were reduced after each dilation. **(f-o)** Closed and open configurations of the valved conduits before and after each dilation showing leaflet coaptation and opening. Scale bars = 10 mm.

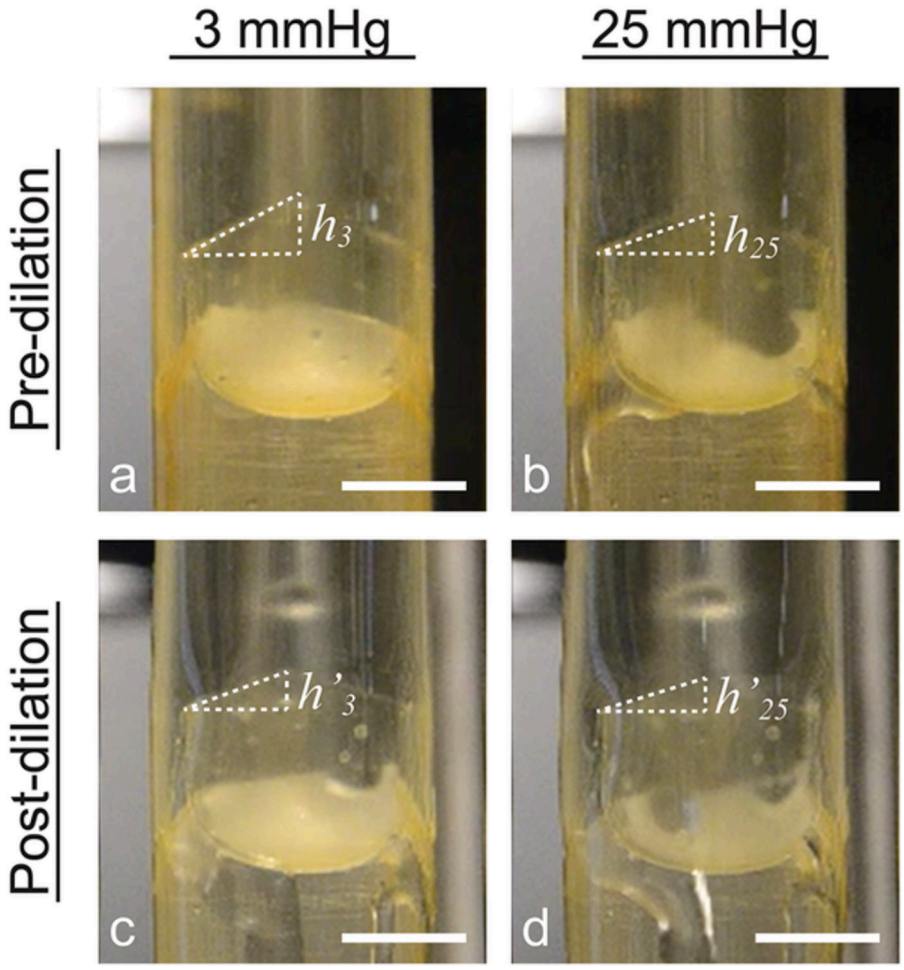

Figure 6. Effect of balloon dilation on initial increased leaflet coaptation height

Images of valved conduits in the pre-dilation state **(a,b)** and post-dilation state **(c,d)** schematically illustrating changes in coaptation height after balloon dilation **(a→c, b→d)** and with increased pressure **(a→b, c→d)**. At a small pressure of 3 mmHg, the increased coaptation height h_3 in the pre-dilation valve **(a)** is greater than the corresponding coaptation height h'_3 in the post-dilation valve **(c)**. An increase in pressure from 3 mmHg to 25 mmHg also leads to apparent reductions in coaptation height h_{25} of a pre-dilation valve **(b)** and in coaptation height h'_{25} of a post-dilation valve **(d)**. Scale bars = 10 mm.

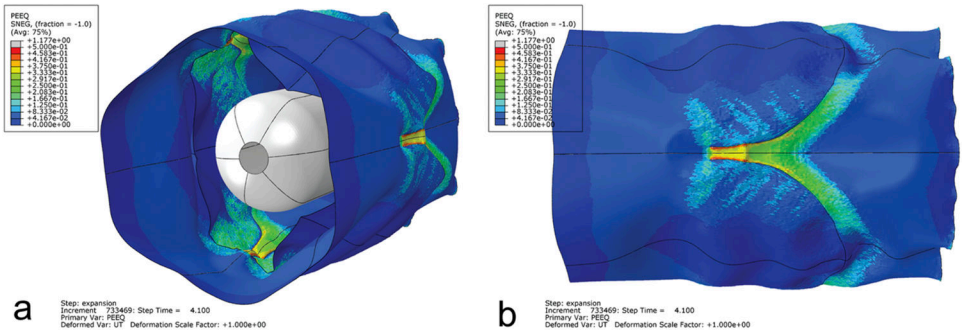

Figure 7. Permanent deformation in the valved conduit predicted by the simulation of the balloon dilation

The device is shown in the final unpressurized, post-dilation configuration. The distribution of permanent deformation is represented by the colored equivalent plastic strain (PEEQ) contours. The colors from blue to red represent increasing amounts of permanent deformation. (a) Angled view showing the valve leaflets and deflated balloon within the conduit. (b) Side view of the conduit exterior. The distribution of permanent deformation was non-uniform throughout the valve region, with the magnitude of deformation being greatest near the commissures. Scale factor of deformations = 1.

Table 1.

***In vitro* test data.**

Hydrodynamic data was recorded over 10 consecutive cardiac cycles (mean ± s.d.). Provided are the maximum RF permitted and minimum EOA required for prosthetic valves in the aortic position per ISO 5840-2:2021, although there are no performance requirements for the pulmonic position.

		Mean arterial pressure [mmHg]	Regurgitant fraction [%]	Mean positive pressure differential [mmHg]	Effective orifice area [cm^2]	Coaptation height (@3mmHg) [mm]	Coaptation height (@25mmHg) [mm]	Final diameter [mm]
Device #1	Pre-dilation	15.0 ± 0.1	2.3 ± 0.2	15.8 ± 1.6	1.14 ± 0.02	$h_3 = 2.92$	$h_{25} = 2.17$	22.00
	Post-dilation *	15.1 ± 0.1	2.5 ± 0.1	14.8 ± 0.0	1.23 ± 0.01	$h_{3,e} = 1.81$	$h_{25,e} = 1.68$	23.00
	2nd Post-dilation **	15.1 ± 0.1	4.5 ± 0.5	9.7 ± 0.2	1.66 ± 0.01			24.56
Device #2	Pre-dilation	15.1 ± 0.1	1.7 ± 0.2	12.0 ± 0.2	1.46 ± 0.01	$h_3 = 2.07$	$h_{25} = 1.97$	22.00
	Post-dilation *	15.0 ± 0.1	2.5 ± 0.1	11.0 ± 0.1	1.51 ± 0.01	$h_{3,e} = 1.49$	$h_{25,e} = 1.38$	22.77
	2nd Post-dilation **	14.9 ± 0.2	4.8 ± 0.4	9.2 ± 0.1	1.64 ± 0.01			24.19
Device #3	Pre-dilation	15.0 ± 0.1	2.0 ± 0.2	9.9 ± 0.4	1.41 ± 0.01	$h_3 = 2.70$	$h_{25} = 2.21$	22.00
	Post-dilation *	14.9 ± 0.1	2.8 ± 0.3	9.4 ± 0.0	1.45 ± 0.01	$h_{3,e} = 2.49$	$h_{25,e} = 2.06$	23.54
Device #4	Pre-dilation	15.1 ± 0.1	3.0 ± 0.1	10.6 ± 0.1	1.63 ± 0.01	$h_3 = 2.85$	$h_{25} = 2.31$	22.00
	Post-dilation *	15.1 ± 0.1	3.9 ± 0.2	8.8 ± 0.2	1.66 ± 0.01	$h_{3,e} = 2.65$	$h_{25,e} = 2.19$	23.71
ISO 5840-2 standards	22 mm valve	-	≤ 10	-	≥ 1.15	-	-	-
	23 mm valve	-	≤ 10	-	≥ 1.25	-	-	-
	24 mm valve	-	≤ 10	-	≥ 1.35	-	-	-

* Post-dilation: Devices were dilated to 40 mm.

** 2nd Post-dilation: Devices were dilated to 44 mm.